Carbohydrate Polymers 313 (2023) 120880

Contents lists available at ScienceDirect

Carbohydrate Polymers

journal homepage: www.elsevier.com/locate/carbpol

Molecular weight and gut microbiota determine the bioavailability of orally administered hyaluronic acid

Matěj Šimek [a,*], Kristýna Turková [b,c], Martin Schwarzer [e], Kristina Nešporová [a], Lukáš Kubala [b,c,d], Martina Hermannová [a], Tereza Foglová [a], Barbora Šafránková [a], Martin Šindelář [c,d], Dagmar Šrůtková [e], Sofia Chatzigeorgiou [a,f], Tereza Novotná [e], Tomáš Hudcovic [e], Vladimír Velebný [a]

[a] Contipro a.s., Dolní Dobrouč 401, 56102 Dolní Dobrouč, Czech Republic
[b] International Clinical Research Center, St. Anne's University Hospital Brno, Brno, Czech Republic
[c] Institute of Biophysics of the Czech Academy of Sciences, Brno, Czech Republic
[d] Institute of Experimental Biology, Faculty of Science, Masaryk University, Brno, Czech Republic
[e] Laboratory of Gnotobiology, Institute of Microbiology of the Czech Academy of Sciences, Nový Hrádek, Czech Republic
[f] Institute of Immunology and Microbiology, 1st Faculty of Medicine, Charles University, Prague, Czech Republic

ARTICLE INFO

Keywords:
Microbiota
Hyaluronan
Metabolism
Bioavailability
Digestion
Oligosaccharides

ABSTRACT

The ability of hyaluronan as a dietary supplement to increase skin moisture and relieve knee pain has been demonstrated in several clinical studies. To understand the mechanism of action, determining hyaluronan's bioavailability and *in vivo* fate is crucial. Here, we used ^{13}C-hyaluronan combined with LC–MS analysis to compare the absorption and metabolism of oral hyaluronan in germ-free and conventional wild-type mice. The presence of *Bacteroides spp.* in the gut was crucial for hyaluronan absorption. Specific microorganisms cleave hyaluronan into unsaturated oligosaccharides (<3 kDa) which are partially absorbed through the intestinal wall. The remaining hyaluronan fragments are metabolized into short-chain fatty acids, which are only metabolites available to the host. The poor bioavailability (~0.2 %) of oral hyaluronan indicates that the mechanism of action is the result of the systematic regulatory function of hyaluronan or its metabolites rather than the direct effects of hyaluronan at distal sites of action (skin, joints).

1. Introduction

Hyaluronan (HA) is a simple repeating disaccharide polymer, consisting of glucuronic acid (GlcA) and *N*-acetylglucosamine (GlcNAc), which is found in all vertebrate tissues as an essential component of the extracellular matrix. (Rodrigues et al., 2015) In the human body, HA is most abundant in the knee joint, articular cartilage, and skin, where it acts as a lubricant, shock absorber, and moisturizer (Gupta et al., 2019). HA metabolism is highly efficient and involves a number of enzymes. In humans, HA is synthesized at the cell surface by HA synthases 1–3 (HAS1–3) most commonly with a molecular weight (M_w) of 1–8 MDa (Cowman et al., 2015) and is degraded by different hyaluronidases (HYAL1, HYAL2, PH-20, CEMIP, CEMIP2) (Sindelar et al., 2021). Apart from homeostatic and filling functions, HA is implicated in cell proliferation, adhesion and migration, triggering a range of signalling pathways by interacting with cell-surface receptors and binding molecules (*e.g.* CD44, layilin, LYVE-1) (Kobayashi et al., 2020).

HA had been used as a dietary supplement for many years for its anti-inflammatory properties and for its ability to increase skin moisture and to relieve knee chronic pain (Pan et al., 2021). Although many clinical studies have demonstrated the beneficial effect of orally-administered HA (Kawada et al., 2014; Oe et al., 2016), inconsistent information is available regarding its bioavailability and mechanism of action. It is suggested that a high-M_w of HA prevents its free transit through the intestinal wall. However, the gastrointestinal tract harbours a complex population of microorganisms, the gut microbiota, containing enzymes capable of cleaving HA into shorter fragments (Ndeh et al., 2020), which can then be more easily absorbed by the host intestinal epithelium (Sato et al., 2020). Gut microbiota may thus act as a crucial mediator of the absorption of orally administered HA. Furthermore, HA may serve as a

* Corresponding author.
E-mail address: matej.simek@contipro.com (M. Šimek).

https://doi.org/10.1016/j.carbpol.2023.120880
Received 1 February 2023; Received in revised form 9 March 2023; Accepted 30 March 2023
Available online 1 April 2023

substrate for gut microbiota (Pan et al., 2021) and thus modulate the composition of the microbial community (Mao et al., 2021), which may have a beneficial impact on the host. Considering the possible mechanisms, several suggestions have been made: a) HA is absorbed and has a direct effect at the site of action (skin, joints) (Oe et al., 2014), b) HA or its fragments in the intestine or organism trigger the specific cell response (Kolar et al., 2015), c) further metabolites of HA in the intestine or in the organism trigger the specific cell response. However, to identify the mechanism of action of orally administered HA, it is crucial to first determine its bioavailability and *in vivo* fate. The results of previous studies showed that HA (~1 MDa, ^{99m}Tc or ^{14}C labelled) orally administered to rats and dogs was distributed throughout the blood, skin, and joints (Balogh et al., 2008) and bioavailability was estimated to be over 16 % (Oe et al., 2014). Conversely, other studies reported that orally administered HA (~1 MDa, native) (Asari et al., 2010) or ^{99}Tc/^{14}C labelled (Laznicek et al., 2012) was not distributed in the body at all. These discrepancies may be attributed to artificial results of techniques employing radioactive or fluorescent probes (Svanovsky et al., 2008). To overcome these drawbacks, we recently introduced ^{13}C labelling in combination with sensitive LC-MS analysis in order to investigate HA metabolism after its application *via* an intravenous route (Šimek et al., 2021).

The aim of this study is to determine by means of unique ^{13}C-labeling technology how HA passes through the gastrointestinal tract, how it is metabolized and distributed in the body, and resolve the discrepant findings about its bioavailability. We hypothesize that bioavailability of HA depends on M_w, that is reducing during the pass of gastrointestinal tract. Additionally, we want to resolve if HA could really serve as a joint or skin nutrition or its clinically proved effects may be attributed to different therapeutic mechanism. The answers to these questions may provide new perspectives on the *in vivo* fate and mechanism of action of orally administered HA.

2. Material and methods

2.1. Materials

^{13}C-labelled form of Nutrihyl® (high-M_w HA) was prepared biotechnologically from D-glucose (U—^{13}C, 99 %) (Cambridge Isotope Laboratories, Tewksbury, USA) by Contipro (Dolní Dobrouč, Czechia). Acid hydrolysis was used for the preparation of low-M_w HA (15 kDa). The solution of high-M_w ^{13}C-HA (10 mg ml^{-1}) was acidified by sulfuric acid to pH 3.0 and then heated at 100 °C for 240 min. After cooling down to room temperature, solutions were neutralized by sodium hydroxide solution. Prior to lyophilization, the HA solution was purified and concentrated by active carbon filtration and ultrafiltration. ^{13}C-labelled unsaturated HA disaccharide (ΔAN2) was prepared by enzymatic degradation of high-M_w ^{13}C-HA by lyase from *Streptococccus pneumoniae* provided by Contipro (Dolní Dobrouč, Czechia). The enzyme (133 UI mg^{-1}) was added to solution of high-M_w ^{13}C-HA (10 mg ml^{-1}) and samples were incubated for 3 h at 37 °C. Afterwards, the mixture was heated for 10 min at 100 °C and filtered using centrifugal filters with an M_w (cut off 2 kDa). The distribution of M_w, the efficiency of the stable isotope labelling of ^{13}C-HA and mass spectrum of ^{13}C-ΔAN2 is displayed in S.Fig. 1. ^{13}C NMR analysis of high-M_w ^{13}C-HA was already published by (Šimek et al., 2021). The standards of even-numbered saturated (type AN_n) and unsaturated (type ΔAN_n) and odd-numbered (type AA_n and NN_n) oligosaccharides of HA (>95 %) were obtained from Contipro (Dolní Dobrouč, Czechia). The list of standards is summarized in S. Table 1. Oligosaccharides are labelled according to commonly used nomenclature (Blundell & Almond, 2006) where number (n) represents the number of building blocks of glucuronic acid (A) and *N*-acetylglucosamine (N). AN, NA, AA describe monosaccharide units at the ends of oligosaccharide chains, Δ stands for the double bond in the structure of the monosaccharide unit at the nonreducing end of the oligosaccharide chain.

Biotin-labelled HA (400 kDa M_w/M_n 1.67, with no fragments lower than 130 kDa) was prepared from native HA (Contipro. Dolní Dobrouč, Czechia) according to (Kessler et al., 2018). The M_w of HA and its distribution were determined by SEC-MALLS as described previously (Čožíková et al., 2017). A mixture of biotin-labelled HA oligosaccharides was prepared from the biotin-labelled HA by means of enzymatic depolymerization with bovine testicular hyaluronidase (EC 3.2.1.35, 2074 U mg^{-1}) (Finepharm, Jelenia Góra, Poland). 300 U mg^{-1} of enzyme was added to the solution of biotin-labelled HA (1 mg ml^{-1}) in acetate buffer (0.05 M, pH 5.4) and the mixture was incubated for 24 h at 37 °C. Afterwards, the mixture was heated for 5 min at 100 °C and filtered using centrifugal filters with an M_w (cut off 2 kDa). Biotin-labelled oligosaccharides were analysed by LC-MS (S.Fig. 3). The main components of the biotin-labelled oligosaccharide mixture were AN4 and AN6 with one molecule of biotin attached. The abundance of other oligosaccharides was estimated to be <2 %. The content of free biotin was determined by LC-MS to be <0.01 %. The same procedure of enzymatic degradation was used for the preparation of mixture of ^{13}C-oligosaccharides which were derived from high-M_w ^{13}C-HA. ^{13}C-labelled oligosaccharides were analysed by MALDI-MS (S.Fig. 4) and by LC-MS (Fig. 3F).

2.2. Pharmacokinetic studies

Conventional female C57Bl/6 J mice (wild-type; WT), 4 weeks of age, were obtained from the laboratory of the Animal Breeding and Experimental Facility of the Faculty of Medicine (Masaryk University, Brno, Czechia) and Anlab (Prague, Czechia). The experiments were approved by the Animal Care Committee of the Czech Academy of Sciences (protocol n. 9/2019) and were in accordance with the EU and NIH Guide for the Care and Use of Laboratory Animals. The mice were co-housed and randomly mixed for 4 weeks in individually ventilated cages with *ad libitum* access to sterile food (25 kGy irradiated SSNIFF mouse breeding extrudate diet V1126–000) and sterile drinking water in the certified clean animal facility of the Institute of Biophysics of the Czech Academy of Sciences, Brno, Czechia with a controlled climate and light/dark cycle (12 h/12 h). The institute is authorized for the use of experimental animals (file number:16OZ22300/2019–18,134; ID:43049/2020-MZE-18134). After 4 weeks, the eight-week-old mice (18-20 g in weight) were randomly divided into experimental groups. Female C57Bl/6 (germ free; GF) mice (8–10 weeks), bred in the Laboratory of Gnotobiology (Nový Hrádek, Czechia) for >10 generations, were kept under sterile conditions in positive pressure Trexler-type plastic isolators on sterile Espe LTE E-002 bedding (Abedd, Kalnciems, Latvia), exposed to 12 h light/dark cycles at a temperature of 22 ± 2 °C and 40 %–60 % humidity, and supplied with autoclaved tap water and sterile food *ad libitum*. The experiments with GF mice were carried out at certified animal facility (ID: 66020/2020-MZE-18134, file number: 17OZ26090/2020–18,134), approved by the Animal Care Committee of the Czech Academy of Sciences (protocol n. 31/2020) and were in accordance with the EU and NIH Guide for the Care and Use of Laboratory Animals. Axenicity was assessed every two-weeks by confirming the absence of bacteria, mold, and yeast by the aerobic and anaerobic cultivation of mouse feces and swabs from the isolators in VL (Viande-Levure), Sabouraud-dextrose, and meat-peptone broth and by subsequent plating on blood, Sabouraud, and VL agar plates. The HA of six different forms – the oligosaccharides ^{13}C-ΔAN2, AN4, ΔAN8, and ΔAN16, and 15 kDa ^{13}C-HA and 1600 kDa ^{13}C-HA was perorally administrated in a physiological saline solution by oral gavage (100 μl or 300 μl; 10 mg ml^{-1}). The administered dose was 50 mg kg^{-1}; the high-M_w HA and ΔAN2 were also dosed at 150 mg kg^{-1}. At nine time points – 0.5, 1, 2, 4, 8, 12, 24, 48 and 72 h after the application of HA (3 animals per each treatment and time point) –, mice were anesthetized by the inhalation of isoflurane, and blood, organs, and tissues were collected. The groups of mice (3 animals per each treatment and time point) were housed in metabolic cages for 24, 48, and 72 h and excrement was

sampled 4, 8, 24, 32, 48, 56 and 72 h after HA application. Plasma was separated by centrifugation (450 *g*/10 min). Organs and tissue were immediately frozen in liquid nitrogen and stored at −80 °C until analysis.

2.3. Long-term supplementation

Thirty conventional WT female C57Bl/6 J mice, 4 weeks of age, were obtained from Anlab (Prague, Czechia). The experiments were approved by the Animal Care Committee of the Czech Academy of Sciences (protocol n. 9/2019) and were in accordance with the EU and NIH Guide for the Care and Use of Laboratory Animals. The mice were co-housed and randomly mixed for 4 weeks in individually ventilated cages with *ad libitum* access to sterile food and sterile drinking water in the certified clean animal facility of the Institute of Biophysics of the Czech Academy of Sciences, Brno, Czechia with a controlled climate and light/dark cycle (12 h/12 h). After 4 weeks, eight-week-old mice (18-20 g in weight) were randomly divided into 10 groups ($n = 3$). Eight of the groups were assigned to the following supplementations (2 groups to 1 supplementation): HA high dose (2.5 mg ml^{-1}, 1600 kDa), HA low dose (0.25 mg ml^{-1}, 1600 kDa), pectin from citrus peel (2.5 mg ml^{-1}, Santa Cruz Biotechnology, Dallas, USA), and GlcNAc (2.5 mg ml^{-1}, Merck, Darmstadt, Germany), while the two remaining groups acted as control (drinking water). All supplements were administrated as a sterile solution in drinking water. The bottles with drinking water plus the supplement were changed daily (HA high dose, HA low dose) or every other day (pectin, GlcNAc, water). The amount of consumed drinking water with supplement per cage was monitored daily by weighing on lab scales. After 28 days, mice were anesthetized by isoflurane inhalation and the content of the cecum was collected under sterile conditions, weighed, and frozen at −80 °C.

2.4. In vitro degradation of ^{13}C-HA by cecal content from oMM^{12} colonized mice

Oligo-Mouse-Microbiota (oMM^{12}) strains were obtained from the DSMZ - German Collection of Microorganisms and Cell cultures GmbH. The bacterial strains were grown in an anaerobic chamber (Concept 400, Ruskinn Technology LTD, Bridgend, UK) filled with a gas mixture (7 % H_2, 10 % CO_2, 83 % N_2) (Linde, Dublin, Ireland) in Anaerobic Akkermansia medium, as described previously (Eberl et al., 2020). 1 ml mixture aliquots of grown strains were frozen at −80 °C until used to establish oMM^{12} gnotobiotic mouse line as described previously (Eberl et al., 2020). Six-week-old oMM^{12}-colonized mice were sacrificed by cervical dislocation, and the cecum was removed and transferred to an anaerobic chamber (Concept 400, Ruskinn Technology LTD, Bridgend, UK) filled with a gas mixture (7 % H_2, 10 % CO_2, 83 % N_2) (Linde) at a temperature of 37 °C. The content of the cecum was transferred to a 15 ml test tube and diluted 1:1 with PBS with 0.05 % L-cystein hydrochloride (pH 6.8, Merck, Darmstadt, Germany). Afterwards, a solution of high-M_w HA (10 mg ml^{-1}, 1600 kDa) was added to achieve an HA concentration of 500 μg ml^{-1}. After throughout mixing, 50 μl of sample was withdrawn at 4 time points (15, 30, 60 and 120 min). Immediately after withdrawal, 200 μl of chilled methanol (−80 °C) was added and samples were then frozen in liquid nitrogen and stored at −80 °C until processed for LC-MS analysis (2.12). The experiments were carried out at certified animal facility (ID: 66020/2020-MZE-18134, file number: 17OZ26090/2020–18,134), approved by the Animal Care Committee of the Czech Academy of Sciences (protocol n. 31/2020) and were in accordance with the EU and NIH Guide for the Care and Use of Laboratory Animals.

2.5. Application of HA into jejunal loops

Female 8-week-old germ-free C57Bl/6 mice were deprived of food for 16 h before surgery (with free access to water). Mice were anesthetized by the intraperitoneal administration of a ketamine/xylazine mixture. Afterwards, laparotomy was performed and 2 cm jejunal loops were created with nylon ligatures. ^{13}C-high-M_w HA, a ^{13}C-oligosaccharide mixture, 400 kDa biotin-labelled HA, and a biotin-labelled oligosaccharide mixture at a concentration of 10 mg ml^{-1} in PBS were injected into jejunal loops through a gauge needle (100 μl). After surgery, the jejunal loop was returned to the abdominal cavity, which was then sutured, and the mouse was placed on heated pad (37 °C). After 2 h, the mouse was euthanized, the abdominal cavity was re-opened, and the jejunal loop was removed and placed in fixative solution (S.Met. 1). The distribution of ^{13}C-oligosaccharides was determined by MALDI-MS imaging (S.Met. 2) and distribution of biotin-labelled HA was determined by confocal microscope (S.Met. 1). The experiments were approved by the Animal Care Committee of the Czech Academy of Sciences (protocol n. 18/2019) and were in accordance with the EU and NIH Guide for the Care and Use of Laboratory Animals. The institute is authorized for the use of experimental animals (ID: 66020/2020-MZE-18134, file number: 17OZ26090/2020–18,134).

2.6. Cell line cultivation and ^{13}C-HA cell uptake

The Caco-2 human colon adenocarcinoma epithelial cell line was cultured according to the manufacturer's instructions in EMEM medium (30–2003, ATCC) supplemented with 10 % FBS (Capricorn Scientific, Ebsdorfergrund, Germany) and 1× penicillin/streptomycin (Biosera, Cholet, France). Cells were seeded on a 6-well plate (350,000 cells/well) for 24 h (37 °C, 5 % CO_2, 95 % humidity) and afterwards media were exchanged for media containing ^{13}C-HA (250 μg ml^{-1}). After 48 h of cultivation, the media were collected and frozen (−80 °C), along with the sterile PBS that was used for washing cells 5 times. To determine ^{13}C-HA content in the cells, 150 μl of cold demineralized water was added to each well and cells were scraped off and transferred to a test tube.

2.7. Quantification of ^{13}C-HA

Quantification of ^{13}C-HA was carried out according to the validated method described by (Šimek et al., 2019). Briefly, AN2 as internal standard together with actinase E (Merck Darmstadt, Germany) were added to the samples and samples were incubated for 3 h at 45 °C. Then, HA lyase from *Streptococcus pneumoniae* (Contipro, Dolní Dobrouč, Czechia) was added and samples were incubated for 30 min at 37 °C. Finally, a chloroform/methanol mixture (900 μl, 4:1, *v*/v) was added, the samples were centrifuged (10,000 *g*/2 min), and the aqueous phase was used for analysis. 1 μl of sample was injected into an Atlantis Premier BEH C18 AX column (50 × 2.1 mm, 1.7 μm) (Waters, Milford, USA) maintained at 25 °C. The mobile phases consisted of 0.1 % formic acid in water (*v*/v) and methanol. The flow rate was set at 0.4 ml min^{-1} and the following gradient of methanol was applied: 0–40 % from 0.5 to 2.5 min, 40–70 % from 2.5 to 3.5 min, 70–0 % from 3.5 to 4 min, and 0 % for 4–5.5 min. An Acquity UPLC I-class chromatographic system was coupled with a Xevo TQ-XS mass spectrometer (Waters, Milford, USA) equipped with an electrospray ionization source.

2.8. Molecular weight of ^{13}C-HA and its distribution

The M_w distribution of ^{13}C-HA in stomach, small intestine, cecum, and colon contents was determined by size exclusion chromatography similarly as described previously (Šimek et al., 2021). 100 μl of sample was injected into two series-connected PL aquagel−OH 40 (300 × 7.5 mm, 8 μm) and PL aquagel−OH 20 (300 × 7.5 mm, 5 μm) columns (Agilent, Santa Clara, USA) which were eluted with 0.15 mol l^{-1} sodium chloride at 1 ml min^{-1} and 40 °C. Twenty fractions (5th–25th minute of elution) were collected and ^{13}C-HA was quantified in each fraction by LC-MS (see Section 2.7).

2.9. Metabolomic analyses

Low-M_w metabolites from 100 µl of cultivated cecum content, tissue homogenates, cell lysates, and cultivation media were extracted with 400 µl of chilled (−80 °C) methanol. Methanolic extracts were dried under a stream of nitrogen and dissolved in 100 µl of 0.1 % formic acid or 60 % isopropanol (*v*/v) for analysis by means of reversed-phase chromatography (RPLC) or hydrophilic interaction chromatography (HILIC), respectively.

A Vanquish Horizon UHPLC system coupled with an Exploris 240 (Thermo Fisher Scientific) mass spectrometer equipped with an electrospray ionization source was used. RPLC was performed according to (Körver-Keularts et al., 2018). Basic HILIC was performed according to (Shi et al., 2019). Metabolites were detected in negative ion mode, utilizing an ion transfer tube temperature of 350 °C, a sheath gas pressure of 60 psi, an auxiliary gas flow of 20, and a spray voltage of 3.5 kV or − 2.5 kV. MS data (*m/z* 70–800) were collected using a dynamic exclusion list and a targeted inclusion list updated in the AcquireX data acquisition mode to achieve optimal metabolite identification in Compound Discoverer 3.3 software (Thermo Fisher Scientific). Metabolites were identified against mz cloud mass spectral library and in-house library of hyaluronan oligosaccharides (mass and retention time). Short chain fatty acids were analysed by GC–MS (S.Met. 6).

2.10. Analysis of oligosaccharides

For the quantification of unsaturated HA oligosaccharides (ΔAN 2,8,10,12,14,16; ≥ 95 %), a mixture of internal standards (saturated HA oligosaccharides AN 2,8,10,12,14,16; 10 µl; 10 µg ml^{-1}; ≥ 95 %) was added to samples of intestinal content, plasma, and urine. Oligosaccharides were obtained from Contipro (Dolní Dobrouč, Czechia). Then, extraction with methanol was performed (see Section 2.9) and the obtained extracts were dissolved in 100 µl of 10 mmol l^{-1} ammonium acetate (pH 5.0). The same buffer and acetonitrile were used as mobile phases for chromatographic separation performed on an Atlantis Premier BEH C18 AX column (50 × 2.1 mm, 1.7 µm) (Waters, Milford, USA), which was maintained at 60 °C. The flow rate was set at 0.4 ml min^{-1} and the following gradient of acetonitrile was applied: 5 % from 0 to 0.5 min, 5–60 % from 0.5 to 5.0 min, 60 % for 5.0–6.0 min, 60–5 % from 6.0 to 6.3 min, and 5 % for 6.3–8.0 min. HA oligosaccharides were analysed on the same system used for the quantification of ^{13}C-HA (see Section 2.7). Measurements were performed in multiple reaction monitoring mode, whereas for each oligosaccharide two transitions were measured (S.Table 1). Typical fragmentations involved formation of glucuronic acid residue (saturated or unsaturated depending on type of oligosaccharides) and cleavage of GlcNAc from reducing end of oligosaccharide. Oligosaccharides were identified according to their retention time and presence of signal of both transitions.

2.11. Data analysis

Differences among samples, tissues and/or individual time points were analysed using linear models with interactions of all involved factors. Post-hoc tests for prespecified pairs were done, correction for multiple comparisons was applied. Generalized linear models were used to compare pharmacokinetic distributions. Level of significance was set to 0.05. All statistical tests were performed in R software.

3. Results and discussion

3.1. Fate of orally-administered HA in conventional WT mice

We used ^{13}C-labelled HA with stable isotopes directly incorporated in the HA structure (S.Fig. 1B) combined with LC-MS analysis (Šimek et al., 2019; Šimek et al., 2021) to determine the kinetics of the permeation of high-M_w HA through the gastrointestinal tract (GIT), its bioavailability, and its distribution in the body. Stable isotope labelling in combination with LC-MS analysis allowed us to resolve *endo*- and exogenous HA, monitor the M_w changes in orally-given HA, and identify its metabolites. ^{13}C-high-M_w HA (1600 kDa) was administered to conventional wild-type (WT) mice by intragastric gavage; this step was followed by the determination of ^{13}C-HA contents in plasma, liver, kidneys, mesenterial lymph nodes, urine, feces, and various parts of the GIT (stomach, small intestine, cecum and colon) at nine different time points from 30 min to 72 h after application (S.Table 2 and 3).

We found that administered ^{13}C- high-M_w HA disappeared from GIT content within 24 h (Fig. 1A). Interestingly, ^{13}C-HA eliminated in feces and urine of WT mice within 72 h was only about 2.2 % and 0.2 % of the administered dose, respectively (Fig. 1B). Therefore, the majority of the high-M_w HA dose was processed within the mouse body. Analysis of the distribution of M_w by offline SEC(LC-MS) showed that the M_w of administered high-M_w ^{13}C-HA gradually decreased during passage through the GIT (Fig. 1D). In more detail, the M_w of ^{13}C-HA shifted from 1600 kDa to approximately 150–600 kDa in the stomach and small intestine and decreased further in both sections over time. Eight hours after administration, ^{13}C-HA was completely depolymerized into short fragments with M_w < 10 kDa. These low-M_w fragments were also the only forms of ^{13}C-HA present in the cecum and colon (Fig. 1E). The reduction in M_w could be caused by several factors. In the stomach, the slight shift in M_w is probably caused by the acidic environment, which partially depolymerizes the HA *via* scission of β(1 → 3) or β(1 → 4) glycosidic bonds (Han et al., 2019; Stern et al., 2007). Further depolymerization in the cecum and colon may be associated with enzymatic cleavage by hyaluronidases in the intestinal wall or HA lyases encoded by gut microbiota that abundantly populate this part of GIT (Yilmaz et al., 2021).

3.2. Origin and nature of HA fragments in the GIT

To identify the nature and origin of short HA fragments in the upper and lower parts of the GIT, an LC-MS analysis of GIT content was employed. Short HA fragments were identified as unsaturated even-numbered oligosaccharides (Fig. 1E), which can be only produced by bacterial and bacteriophage HA lyases (Sindelar et al., 2021). The contents of GIT of WT and GF mice were analysed also for other types of oligosaccharides such as odd-numbered oligosaccharides with GlcA or even-numbered oligosaccharides with GlcNAc at reducing end which can be produced by mammalian hyaluronidases (Sindelar et al., 2021) or by acid hydrolysis at high acid concentrations (Han et al., 2019). However, any of these oligosaccharides were not found in any part of GIT of WT or GF mice. Thus, it can be concluded that the activity of mammalian hyaluronidases nor the acid hydrolysis were not involved in the degradation process and formation of unsaturated fragments. The most abundant oligosaccharide was the unsaturated disaccharide ΔAN2, which accounted for >80 % of HA present in colon contents (Fig. 1E, S. Table 4). The amount of other unsaturated oligosaccharides with 8–20 monosaccharide units accounted only for <4 % of HA present in colon contents.

To confirm the bacterial origin of the observed depolymerization of HA in the GIT, ^{13}C-HA (1600 kDa) was orally administered to germ free (GF) mice and its pharmacokinetics and M_w distribution were inspected. The passage of HA through the GIT was expectedly slower (Fig. 2A); however, this cannot be attributed only to the different metabolization of HA. Passage and elimination kinetics in GF mice are generally slower due to the enlarged cecum (Luczynski et al., 2016) and thicker mucus layer (Johansson et al., 2015). However, even the metabolization of HA in the GIT of GF mice differed significantly. Surprisingly, administered HA crossed the GIT in an almost intact form, with no depolymerization in lower parts of the GIT (Fig. 2C). The LC-MS analysis also did not reveal any unsaturated or other HA oligosaccharides, which clearly indicates that the unsaturated oligosaccharides observed in WT mice came from the bacterial metabolization of HA. As mentioned before, HA can

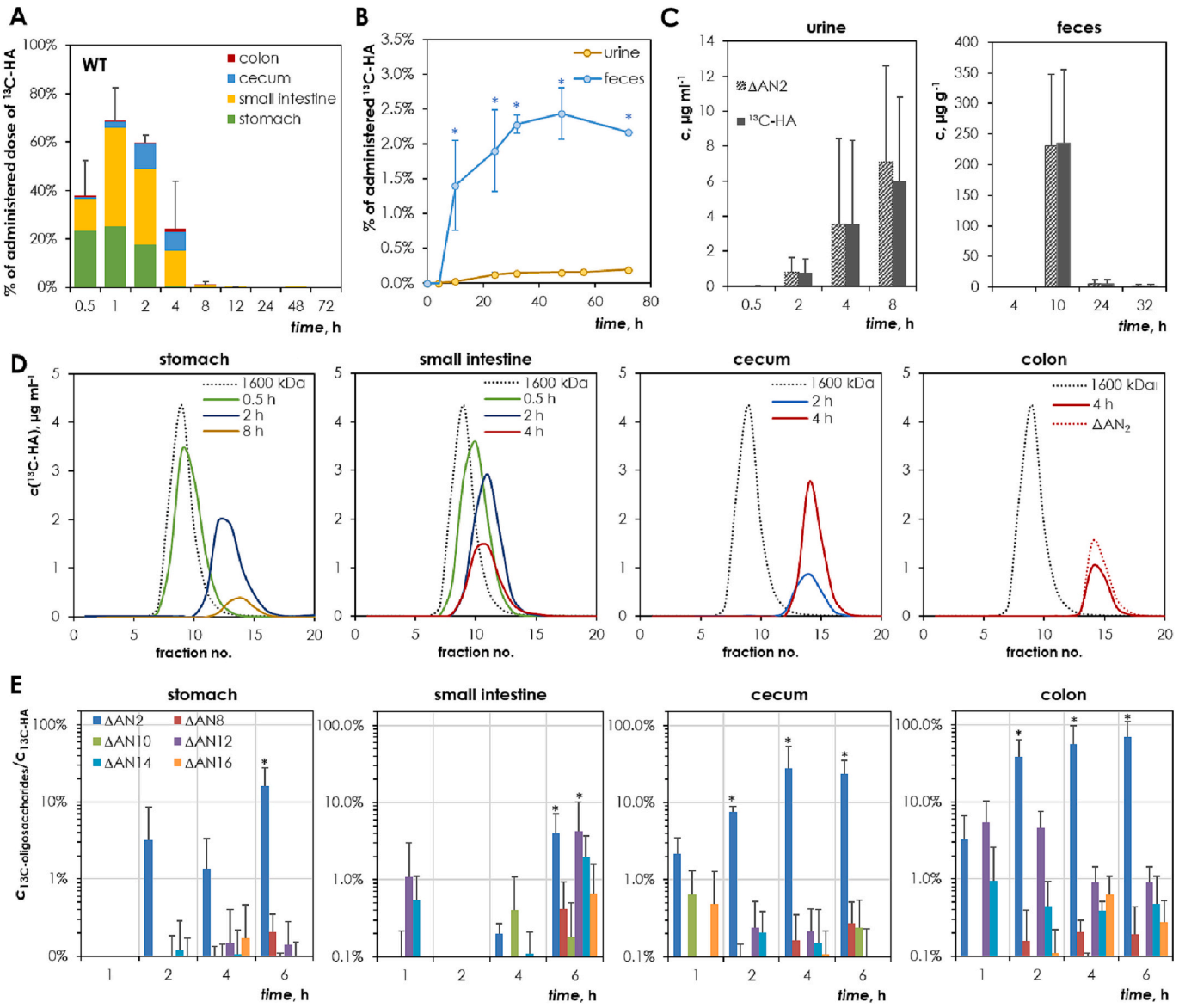

Fig. 1. Pharmacokinetics of high-M_w ^{13}C-HA administered orally to conventional WT mice. A) Amount of ^{13}C-HA in various parts of the GIT and at different time points, B) Elimination of ^{13}C-HA in urine and feces ($n = 3$; compared to samples of feces, $*p < 0.05$), C) Concentration profiles of HA and unsaturated HA disaccharide in urine and feces, D) Changes in M_w distribution of orally administered ^{13}C-HA measured by SEC(LC-MS). The dotted lines are associated with a M_w distribution of 1600 kDa ^{13}C-HA before *p.o.* administration and standard of ΔAN2 in PBS, solid lines represent the M_w distribution of ^{13}C-HA at various time points in various parts of the GIT. The shift of the fraction number to higher values indicates a decrease in M_w., E) Amount of unsaturated oligosaccharides in various parts of the GIT expressed as a ratio between the amount of oligosaccharide and the total amount of ^{13}C-HA ($n = 3$; compared to zero value, $*p < 0.05$). AN describes the type of monosaccharide units at the ends of the oligosaccharide, the number describes the number of monosaccharide units, and Δ stands for the double bond in the structure of the monosaccharide unit at the end of oligosaccharide chain. Only the oligosaccharides ΔAN 2,8,10,12,14, and 16 were quantified due to the availability of standards; however, if these oligosaccharides were present in samples, longer oligosaccharides (ΔAN18 and 20) were also present (S.Fig. 2).

also be depolymerized by acids (Stern et al., 2007); therefore, the acidic environment of the stomach needs to be considered. The acidic environment of the GF mouse stomach (pH 3–4) (McConnell et al., 2008) resulted in a slight decrease in M_w; similar results were also obtained in an *in vitro* experiment with artificial gastric juice with a more human pH of 1.5, where a similar shift in M_w was observed (Fig. 2B). The decrease in M_w in the stomachs of WT mice (Fig. 1D) was more significant due to the presence of stomach microbiota (Wu et al., 2014) which could cause decrease of pH contributing to increased acid degradation of HA (Shimizu et al., 2021). However, the presence of unsaturated oligosaccharides (specific metabolites of bacterial degradation) in stomach (Fig. 1E) and absence of other types of oligosaccharides in stomach and artificial gastric juice indicates that higher depolymerization of HA in stomach of WT mice is caused by bacterial degradation.

To confirm the similarity between WT and GF mice models with respect to HA receptors and HA degrading enzymes in the GIT, the immunohistological analysis of HA-related proteins in the ileum, cecum, and colon was performed. It was found that the distribution and abundance of HA receptors and enzymes was similar in WT and GF mice (S. Fig. 5). Therefore, the observed differences in the pharmacokinetics of HA in WT and GF may be attributed only to anatomical differences and the presence of gut microbiota.

3.3. Penetration of HA fragments through the intestinal wall

To determine which HA fragments can penetrate through the intestinal wall and be available to the host, HA of six different forms (oligosaccharides (ΔAN2, AN4, ΔAN8, ΔAN16), low-M_w HA, high-M_w HA)

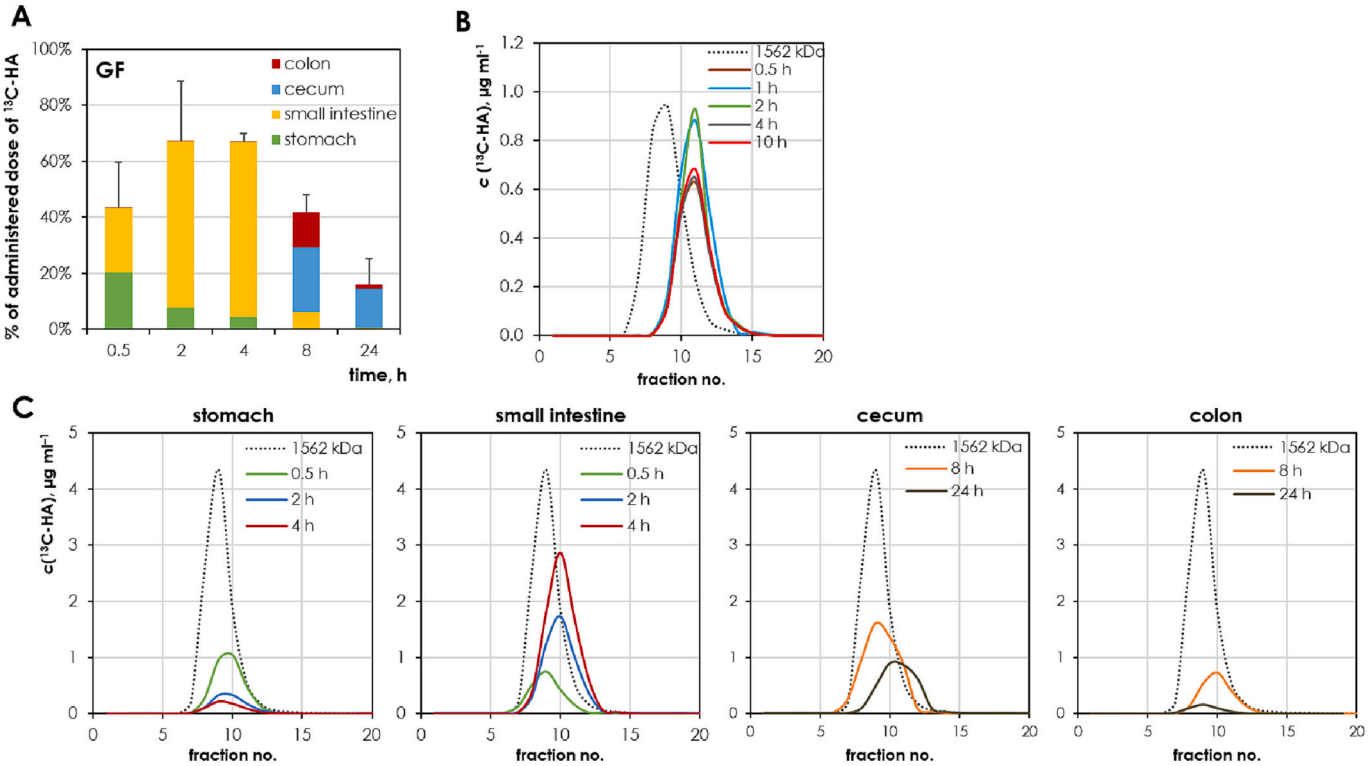

Fig. 2. Pharmacokinetics of high-M_w ^{13}C-HA administered orally to GF mice. A) Amount of ^{13}C-HA in various parts of the GIT at different time points, B) Changes in the M_w distribution of ^{13}C-HA during degradation by artificial gastric juice (pH 1.5), C) Changes in the M_w distribution of orally-administered ^{13}C-HA. The dotted lines are associated with the M_w distribution of administered ^{13}C-HA in PBS; solid lines represent the M_w distribution of ^{13}C-HA at various time points in various parts of the GIT. The shift of the fraction number to higher values indicates a decrease in M_w.

with M_ws (0.38, 0.78, 1.52, 3.03, 15.0 and 1600 kDa) were orally administered to WT mice. The analysis of HA in urine showed that the amount of HA in urine, and, thus, respectively, the bioavailability of oral HA, is inversely related to its M_w (Fig. 3A). Additionally, using LC-MS oligosaccharide analysis, the presence of ΔAN16 (3.03 kDa) in urine after its oral administration was confirmed (S.Fig. 6). This suggest that fragments with $M_w \leq \sim$3 kDa can pass through the intestinal wall, be available to the host, and subsequently be eliminated in urine. These data also correlate with the *in vitro* study by (Hisada et al., 2008), in which the authors observed an inverse relation between the permeability of HA through the Caco-2 cell monolayer and its M_w. Similar results have also been reported by (Sato et al., 2020), the authors observing a significant difference between the absorption of HA fragments of 2 kDa and 8 kDa.

Despite these results indicating that the intestinal absorption of native high-M_w HA is not possible, there are several studies suggesting the possibility of high-M_w HA uptake through the lymphatics (de Souza et al., 2019; Kawada et al., 2014). To resolve this question, biotin- and ^{13}C-labelled middle and high-M_w HA (0.4 and 1.6 MDa) and an oligosaccharide mixture (AN4,AN6,AN8 (M_w < 1.5 kDa)) were injected into jejunal loops of GF mice (Štěpánková et al., 1996). After 2 h, the penetration of HA through the intestinal wall was evaluated by confocal microscopy and MALDI-MS imaging, while the absorption of ^{13}C-HA into portal blood, blood from cardiac puncture, and mesenterial lymphatic nodes was determined by LC-MS. Due to the absence of intestinal microbiota, the intestinal absorption depended only on the M_w of the administered HA. MALDI-MS imaging together with confocal microscopy revealed the distribution of oligosaccharides in intestinal epithelium 2 h after their administration (Fig. 3B,C); however, biotin-labelled 400 kDa HA did not penetrate into the epithelium and remained intact inside the jejunal loop. This was also confirmed by SEC (LC-MS) analysis of ^{13}C-HA (Fig. 3E). After the administration of oligosaccharides, the ^{13}C-HA concentration in portal blood and mesenterial lymph nodes was 151.2 ± 70.8 ng ml^{-1} and 321.3 ± 179.0 ng g^{-1}, respectively. The concentration of ^{13}C-HA after the administration of high-M_w HA was below the limit of quantification (10 ng ml^{-1}). These data correspond to our pharmacokinetic studies with GF and WT mice (S.Table 3). Similar *in vitro* observations were made by (Kim et al., 2018) on mouse intestinal organoids, where 35 kDa HA in contrast to 2000 kDa HA penetrated into epithelial cells. Thus, high-M_w HA is not absorbed in its intact form and microbial degradation into short fragments (< ~3 kDa) is necessary for its absorption from the gut.

HA and its fragments can bind to several HA binding receptors including CD44, LYVE-1, and layilin. Their presence in the intestine was confirmed by several studies (Gracz et al., 2013; Kim & de la Motte, 2020; Kim et al., 2018; Soroosh et al., 2016). Additionally, intestinal epithelial cells contain hyaluronidases (Hyal1, Hyal2 and CEMIP2) (Bouga et al., 2010; Chowdhury et al., 2016; Uhlén et al., 2015). To investigate whether orally-administered HA could be utilized by intestinal epithelium, an *in vitro* study with Caco-2 cells was performed. The Caco-2 cells, commonly used as a model for intestinal absorption, were cultivated for 24 h in medium containing HA of eight different forms: unsaturated (ΔAN2, ΔAN8, ΔAN16) and saturated (AN2, AN8, AN16) oligosaccharides, and low-M_w and high-M_w HA (15 and 1600 kDa). The change in HA concentration at the end of cultivation was negligible, and only a small proportion of the applied HA was found intracellularly (<0.1 %). The uptake was inversely related to the M_w of HA and a significant difference between unsaturated oligosaccharides (~50–90 %) and their saturated analogues (Fig. 3D) was observed. The ability of intestinal mucosa to utilize HA was also tested on jejunal loops of GF mice. However, no decrease in the M_w of applied high-M_w HA (Fig. 3E), no changes in the lengths of the applied oligosaccharides (Fig. 3F), and no HA metabolites in the jejunal loop content or tissue were observed. The abundance and distribution of HA receptors and enzymes in

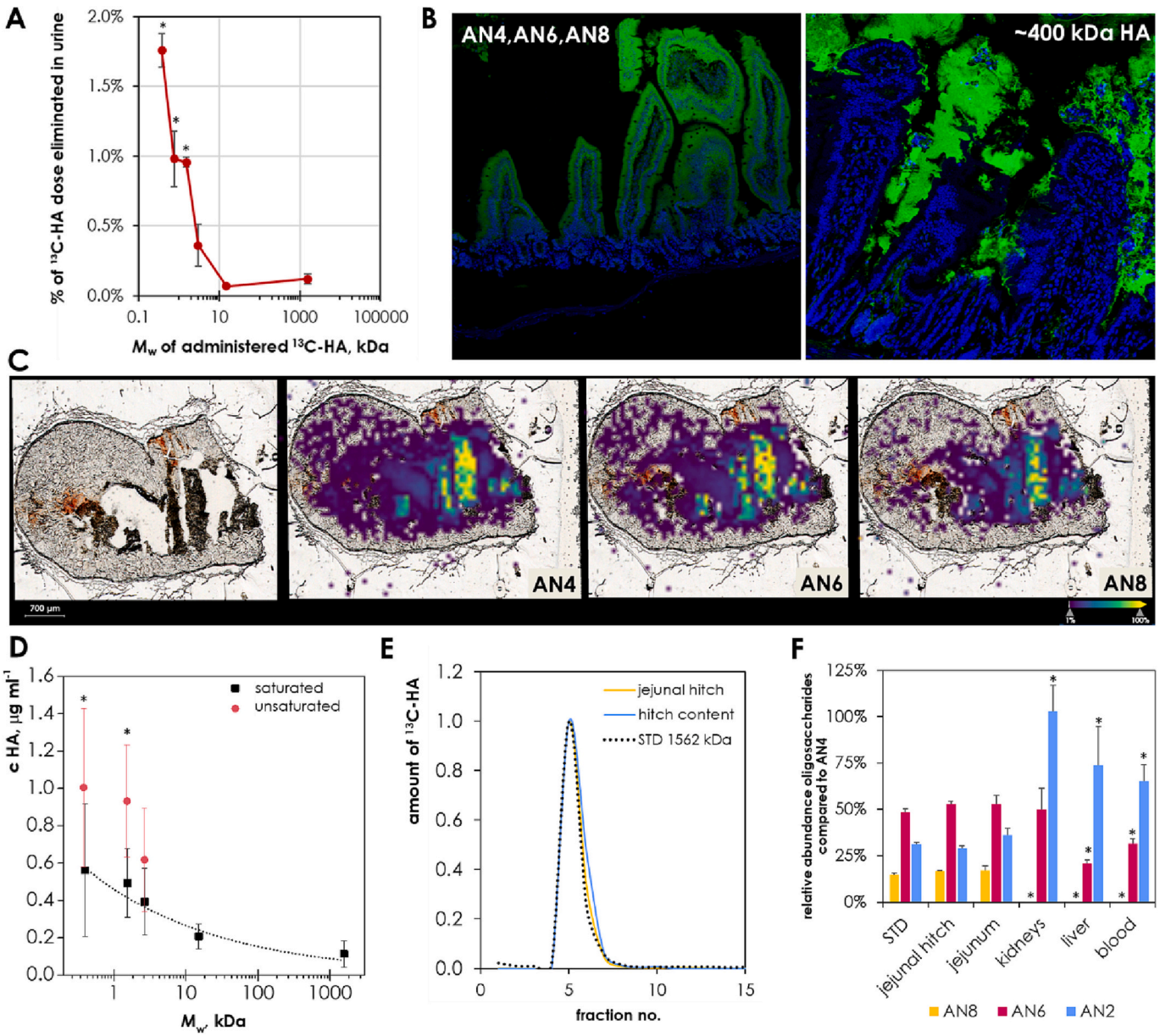

Fig. 3. Absorption and metabolization of oral HA by intestinal epithelium. A) Amount of ^{13}C-HA eliminated in urine as fragments of ^{13}C-HA in dependence on M_w of ^{13}C-HA administered to WT mice ($n = 3$; compared to results for 1600 kDa, $^*p < 0.05$); B) Penetration of biotin-labelled HA in jejunal loops of GF mice 2 h after a mixture of HA oligosaccharides (AN4,AN6,AN8) or middle weight molecular weight HA (M_w 400 kDa) was injected into the loops (green – biotin-HA, blue – cell nuclei) – the specificity of biotin labelling was verified by LC-MS (**S.**Fig. 3); C) MALDI-MS imaging of ^{13}C-HA oligosaccharides 2 h after their administration into the jejunal loop. The distribution of oligosaccharide signal intensity from lowest to highest is represented by a color series (purple-blue-green-yellow). The specificity of ^{13}C labelling was verified by MALDI-MS (**S.**Fig. 4)**;** D) Intracellular concentration of HA after cultivation of Caco-2 cells for 24 h in medium containing saturated or unsaturated oligosaccharides (AN- and ΔAN-type 2,8-,16- mers-), or low- or high-M_w HA at 0.25 mg ml^{-1} ($n = 3$; $^*p < 0.05$); E) M_w distribution of ^{13}C-HA after its incubation for 2 h in jejunal loops of GF mice; F) Relative abundance of saturated oligosaccharides (AN-type 2-,6-,8-mers) compared to AN4 in oligosaccharide mixture administered to jejunal loops of GF mice and in tissue after 2 h of incubation ($n = 3$; compared to standard mixture, $^*p < 0.01$). (For interpretation of the references to color in this figure legend, the reader is referred to the web version of this article.)

jejunum is similar to their abundance and distribution in the rest of the intestine (S.Fig. 5); therefore, HA from intestinal contents is not metabolized by intestinal epithelium, but only by gut microbiota into unsaturated oligosaccharides, which are transported by lymph and the blood stream into the body. The concentrations of HA in portal blood and mesenterial lymph nodes were similar; however, the lymphatic flow rate is much slower (0.2 %) than that of portal blood (Sato et al., 2020). Therefore, it can be concluded that the absorption of HA in blood capillaries is the dominant route of transportation of unsaturated oligosaccharides from the intestine into the body.

3.4. Distribution of absorbed HA in the body

The bioavailability of administered high-M_w HA was practically zero for GF mice, since the concentration of ^{13}C-HA in plasma, urine, and organs was below the limit of detection (<3 ng ml^{-1}) (S.Table 2, 3). In contrast, the plasma concentration of ^{13}C-HA for WT mice was significantly higher (c_{MAX} 140 ng ml^{-1}). The concentration of ^{13}C-HA in other parts of the body was negligible (S.Table 3). The highest concentration of ^{13}C-HA was measured in urine (c_{MAX} 6.0 µg ml^{-1}). The low concentration of ^{13}C-HA in plasma and the relatively high concentration in urine can be explained by the rapid elimination of low-M_w HA fragments

by glomerulus filtration (Šimek et al., 2021). The bioavailability of HA is therefore represented by the amount of ^{13}C-HA absorbed and eliminated in urine, which represented only 0.2 % of the administered dose for high-M_w HA (Fig. 3A). Additionally, ΔAN2 was the only form of absorbed HA present in urine after the administration of high-M_w (1600 kDa) (Fig. 1C) or low-M_w (15 kDa) HA. These results clearly indicate that the depolymerization of HA by gut microbiota into unsaturated oligosaccharides is essential for its absorption into the body; however, even after this process, the bioavailability of HA is still very low.

After 24 h, only about 3 % of the administered dose of high-Mw HA was recovered from the feces, urine, and bodies of WT mice (Fig. 1B, S. Table 2). Therefore, > 97 % of the administered HA was either completely metabolized by the gut microbiota or depolymerized by the gut microbiota to unsaturated oligosaccharides and subsequently absorbed and metabolized in the body to low-M_w metabolites. To determine which was the case, GF and WT mice were fed ^{13}C-ΔAN2 (Fig. 4). The quantification of ΔAN2 in plasma, urine, and body organs showed that the amount of absorbed ΔAN2 for WT and GF mice was similar and very low (<3 % of the administered dose) (Fig. 4B), while only about 1 % of administered ΔAN2 was recovered in feces of WT mice (Fig. 4C). Additionally, no ^{13}C eukaryotic metabolites were observed in the body after the administration of high-M_w ^{13}C-HA, or ^{13}C-ΔAN2. This indicates that regardless of the form of administered HA the majority of dosed HA is metabolized in the GIT and its absorption into the body is very limited. This conclusion correlates with the fact that no metabolization of HA fragments in intestinal epithelium was observed (Fig. 3E, F) and that after the administration of longer oligosaccharides (Fig. 3A), these were absorbed and eliminated in urine predominantly in their intact form (S.Fig. 6).

These findings correlate with previously-published data on the bioavailability of oral HA (Asari et al., 2010; Laznicek et al., 2012; Ma et al., 2015) and oral chondroitin sulphate (Volpi, 2002; Volpi, 2003). Conversely, other studies have reported that HA (~1 MDa, ^{99m}Tc or ^{14}C labelled), orally administered to rats and dogs, was distributed throughout the blood, skin, and joints (Balogh et al., 2008) and that its bioavailability was estimated to be over 16 %(Oe et al., 2014). These discrepancies in the context of our new findings probably result from non-ideal labelling strategies on the part of techniques employing radioactive probes which could not distinguish between free label, labelled high-M_w HA, and its labelled metabolites. In contrast, our stable isotope labelling of HA combined with LC–MS or SEC analysis provides an excellent approach to elucidating HA's *in vivo* fate.

To test the hypothesis that absorbed HA can penetrate deeper into the organism – for example, into skin and joints, where it can act as an anti-inflammatory, lubricating, and humidifier agent – and since we did not observe any significant absorption with a dosage of 50 mg kg^{-1}, we applied high-M_w ^{13}C-HA and ^{13}C-ΔAN2 to WT mice at the highest possible dose of 150 mg kg^{-1}. After the administration of ^{13}C-ΔAN2, the ^{13}C-ΔAN2 was clearly visible in skin and knee joints (Fig. 4D); in contrast, the administration of a high dose of high-M_w HA resulted in only a negligible increase above the baseline. Thus, if HA is administered at high doses and the gut microbiota can efficiently cleave HA, oral HA in the form of ΔAN2, may reach the skin and joints, albeit in very limited amounts (< ~5 ng g^{-1}). Thus, this commonly discussed mechanism of action is very unlikely, since HA absorption is very limited. This is further amplified by the fact that beneficial effects of oral HA are reported for much lower doses (< ~3 mg kg day^{-1}) (Oe et al., 2016) than were used in our pharmacokinetic study.

3.5. Bacterial metabolization of HA

The action of gut microbiota has been shown to be crucial for the bioavailability of orally administered HA. The presence of ΔAN2 in urine (Fig. 1C) after the oral administration of high-M_w HA indicates

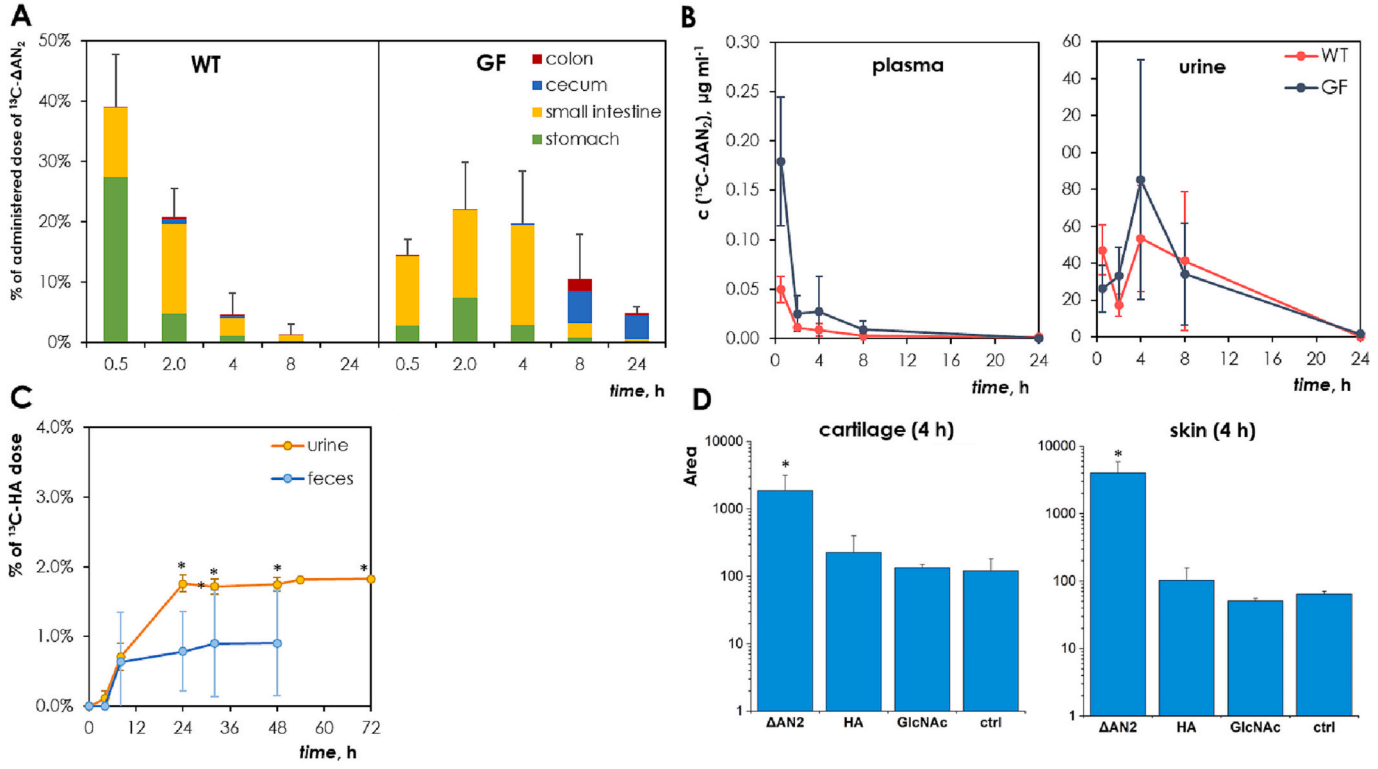

Fig. 4. Pharmacokinetics of orally administered unsaturated HA disaccharide (^{13}C-ΔAN2). A) Amount of ΔAN2 in various parts of GIT and at different time points after its oral administration to WT and GF mice (50 mg kg^{-1}), B) Absorption of orally administered ΔAN2 to plasma and urine of WT and GF mice (50 mg kg^{-1}), C) Elimination of ΔAN2 in urine and feces after its oral administration to WT mice (50 mg kg^{-1}, samples from metabolic cages; $n = 3$, compared to samples of feces, *$p < 0.05$), D) Distribution of ΔAN2 into distal tissues 4 h after administration of a high dose of HA and ΔAN2 (150 mg kg^{-1}). Samples labelled as GlcNAc and ctrl refer to mice which received *N*-acetylglucosamine or water, respectively ($n = 3$; compared to ctrl, *$p < 0.05$).

that ΔAN2 is the product of the cleavage of extracellular or cell-surface bacterial lyases (Ndeh et al., 2020; Oiki et al., 2017). However, there are number of known enzymes which could also participate in the bacterial degradation of HA. To determine other metabolites and reveal possible metabolic changes in the intestine, the contents of the small intestine and cecum of mice colonized with the defined oMM^{12} bacterial mixture were cultivated with high-M_w ^{13}C-HA. The quantification of ^{13}C-HA by LC-MS revealed that the ^{13}C-HA was completely metabolized in cultivated cecal content within 120 min (Fig. 5A). In contrast, ^{13}C-HA in the content of the small intestine was not degraded even after 4 h (data not shown). The oMM^{12} mixture contains five bacterial phyla that are naturally abundant in the murine GIT, such as *Actinobacteria,*

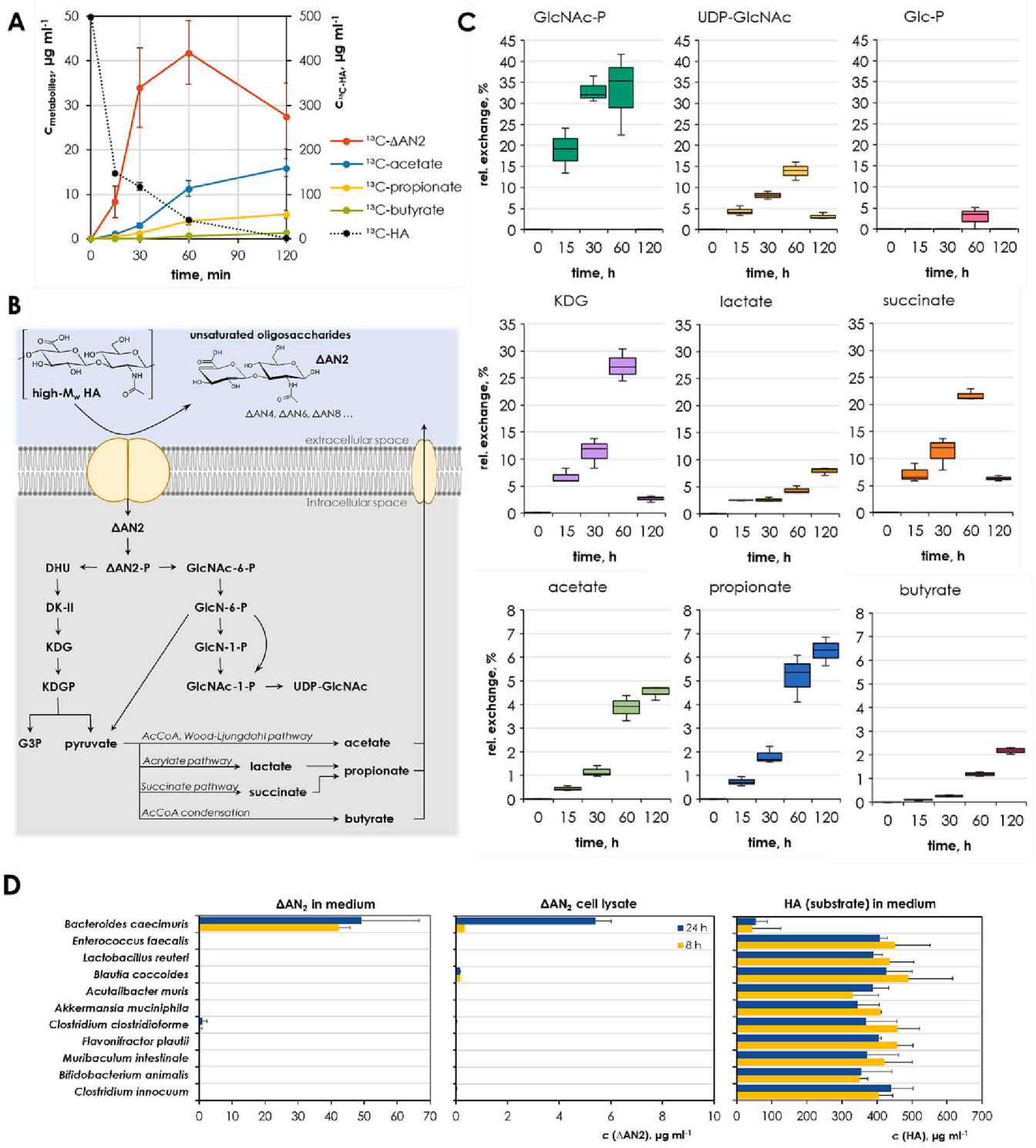

Fig. 5. *In vitro* degradation of ^{13}C-HA by oMM^{12} microbiota. A) Kinetics of ^{13}C-HA degradation and the formation of its metabolites, B) Schematic diagram of bacterial degradation of HA, C) Relative exchanges of ^{13}C in selected metabolites, D) Degradation of HA by isolated bacterial strains of oMM^{12} mixture into unsaturated HA disaccharide (ΔAN2) (S.Met. 3). (ΔAN2-P: 2-Acetamido-2-deoxy-6-phospho-3-O-(4-deoxyhex-4-enopyranuronosyl)hexopyranose, DHU: 4-deoxy-l-threo-5-hexosulose-uronic acid, DK-II: 3-deoxy-d-glycero-2,5-hexodiulosonic acid, KDG: 2-keto-3-deoxy-d-gluconic acid, KDGP: 2-keto-3-deoxy-6-phosphogluconic acid, G3P: glyceraldehyde-3-phosphate, UDP-GlcNAc: uridine diphosphate *N*-acetylglucosamine, GlcNAc: *N*-acetylglucosamine).

Bacteroidetes, Firmicutes, Proteobacteria and *Verrucomicrobia (Eberl et al., 2020)*. *Bacteroides caecimuris* was the only HA cleaving bacteria from the synthetic microbial community of the oMM^{12} mixture (Fig. 5D) and its abundance in the cecum of oMM^{12} mice is significantly higher than in the small intestine (Yilmaz et al., 2021). This corresponds to our *in vivo* data for WT mice (Fig. 1D), suggesting that bacteria-degrading HA are present primarily in the mouse cecum. Generally, 20 % of the *Bacteroides* genome is dedicated to complex glycan metabolism. *Bacteroides spp.* are prominent degraders of glycosaminoglycans, polysaccharides and *N*-glycans; thus, their presence in the intestine is closely related to HA degradation (McKee et al., 2021).

Simultaneously with the decrease in ^{13}C-HA concentration in the cecal content of oMM^{12} mice, the production of ΔAN2 was observed (Fig. 5A, S.Fig. 7). Interestingly, no other unsaturated oligosaccharides were found, even though the ability of *Bacteroides* surface lyase to produce longer unsaturated oligosaccharides was described (Ndeh et al., 2020). Nevertheless, the ^{13}C-label was further identified in several low-M_w metabolites (Fig. 5C). According to the proposed metabolic pathway for gram-positive and gram-negative bacteria (Oiki et al., 2017), ΔAN2 undergoes phosphorylation on GlcNAc and subsequent cleavage into unsaturated GlcA and *N*-acetylglucosamine-phosphate (GlcNAc-P). A high level of incorporation (>25 %) was identified in $C_6H_{10}O_6$, which corresponds to the metabolite of unsaturated GlcA. Similarly, the high incorporation of the ^{13}C-label was observed in GlcNAc-P (>30 %) and uridine diphosphate *N*-acetylglucosamine (UDP-GlcNAc) (>12 %). The high level of incorporation and the number of eight ^{13}C atoms within GlcNAc-P and UDP-GlcNAc indicates that these molecules are formed by direct conversion from ΔAN2 (Fig. 5B), which is in accordance with the suggested metabolic pathway. The metabolization of HA into UDP-GlcNAc implies not only that the HA serves as a source of energy but also that its metabolites could serve as building blocks for the synthesis of complex glycans, which was also recently proven for human liver endothelial cells (Šimek et al., 2021).

The significant incorporation of ^{13}C was also observed within the structures of short chain fatty acids (SCFA) and hydroxy acids (lactate, succinate) (Fig. 5C, S.Fig. 8). SCFA are end products of anaerobic bacterial fermentation and can be formed *via* different metabolic pathways according to the bacterial phyla. The level of ^{13}C-incorporation within the structure of succinate (~20 %) is significantly higher than that within lactate (~7 %); simultaneously, a significant proportion of ^{13}C-succinate and ^{13}C-propionate molecules contains three ^{13}C atoms (S. Fig. 8). These data mean that the majority of propionate is formed *via* the succinate pathway characteristic for *Bacteroides spp.* (Reichardt et al., 2014). A half of ^{13}C-butyrate molecules have 2–4 atoms of ^{13}C, which corresponds to its formation by the butyryl-CoA pathway; the other half contain only 1 atom of ^{13}C, which corresponds to its formation *via* the fixation of ^{13}C-carbon dioxide (S.Fig. 8). These data signify that HA cannot only be cleaved but also utilized by *Bacteroides spp.* and completely metabolized into SCFA and CO_2.

These findings suggest that bacterial metabolites arising from administered HA can be absorbed into the body and have beneficial effects for the host. For example, SCFA can strengthen the function of the gut barrier and have important immunomodulatory functions (Parada Venegas et al., 2019), while UDP-GlcNAc is a substrate in multiple protein glycosylation pathways, thereby widely impacting the proteome (Biwi et al., 2018). To investigate the bioavailability of the identified HA metabolites, metabolomic analyses of plasma and liver of WT mice after *p.o.* administration of high-M_w ^{13}C-HA and ^{13}C-ΔAN2 (150 mg kg^{-1}) were performed. LC-MS analysis revealed that the ^{13}C-label was not incorporated into these metabolites (*e.g.* GlcNAc, UDP-GlcNAc) or these metabolites (*e.g.* KDG, DHU) were not found. These data indicate that intermediate metabolites of the intracellular metabolism of the bacterial degradation of HA are not available to the host. However, this may not be the case with SCFA, end products of the bacterial metabolism of HA, which are effectively absorbed in the colon (Parada Venegas et al., 2019). Significant metabolization of ^{13}C-HA into ^{13}C-SCFA was observed in the cecum and colon (S.Fig. 9), which means that HA supplementation may lead to a significant increase in SCFA contributing to intestinal homeostasis (Parada Venegas et al., 2019).

3.6. Modulation of the cecal microbial community by the long-term administration of HA

The presence of gut microbiota, especially in the cecum, seems to be crucial for the metabolization and absorption of orally administered HA. However, the interactions between HA and gut microbiota are not fully understood and have not been precisely described. Several *in vitro* and *in vivo* studies were conducted to study the modulation of microbial communities by the administration of HA (Bellar et al., 2019; Chaaban et al., 2021; Mao et al., 2021; Pan et al., 2021), but their conclusions are not consistent.

To determine whether a 4-week supplementation with high-M_w HA affects the cecal microbiota composition of healthy WT mice, DNA isolated from cecal contents was amplified in the V3-V4 region of the 16S-rRNA gene, followed by sequencing of the amplified region (S.Met. 4). Together with HA, the effects of GlcNAc and pectin supplementation were studied. The obtained genomics data contained 3,180,588 raw reads; after the removal of unqualified sequences, a total of 2,140,547 raw reads with an average length of 408 bases remained. Principal coordinates analysis showed that the cecal microbiota of HA-treated mice were not altered compared to the control group (S.Fig. 10). Mothur method *get.communitytype* predicted only one metacommunity cluster. No statistical significance in the alpha diversity between groups was observed. Analysis of molecular variance analysis revealed only a slight shift in gut microbiota composition for GlcNAc treatment. Homogeneity of molecular variance analysis did not confirm any significant difference across the tested groups. These results are consistent with literature. The oral administration (140 mg day^{-1}) of 35 kDa HA to healthy human subjects for 4 weeks was found to have no significant effect on microbiome alpha- and beta diversity, and no significantly different operational taxonomic units were revealed throughout the time course (day-0, day-8, and day-28) (Bellar et al., 2019). Similar results were observed by (Mao et al., 2021) with healthy mice and mice with DSS-induced colitis. Once-a-day supplementation with 35 kDa HA did not lead to any significant changes in gut microbiota populations; however, a significant increase in gut microbial diversity was observed.

Overall, the relative abundances of bacterial genera revealed high between- and within-group variation (Fig. 6A) and correspond to high within-group variability in the bacterial degradation products of HA (Fig. 1E). Despite exhibiting high within-group variability, the genera with confirmed HA degradation activity – namely, *Bacteroides* and *Enterococcus (Kawai et al., 2018)* – showed a marked increase in abundance for HA treated groups (Fig. 6B). However, the difference was not statistically significant due to the large sample diversity. Although not visible in taxonomic classification, an increase in some OTUs of the less frequent genera *Anaeroplasma*, *Clostridium_XlVb*, and *Parabacteroides* was observed despite there being no information about their ability to cleave HA found in databases. Similarly, the abundance of *Akkermansia muciniphila* increased after the oral application of HA (Lee et al., 2020; Mao et al., 2021), despite the fact that its ability to degrade HA was not observed in our study (Fig. 5D).

4. Conclusion

In this study, we revealed in detail the pharmacokinetic behavior of orally-administered high-M_w HA in conventional WT and GF mice in order to provide a new perspective on the *in vivo* fate of orally administered HA. As we hypothesized, high-M_w HA is depolymerized during the pass of GIT. However, the main finding is that the depolymerization of orally-administered HA by gut microorganisms is essential for ensuring its bioavailability and is fully dependent on gut microbiota, since in GF animals high-M_w HA is not absorbed at all. Our results clearly

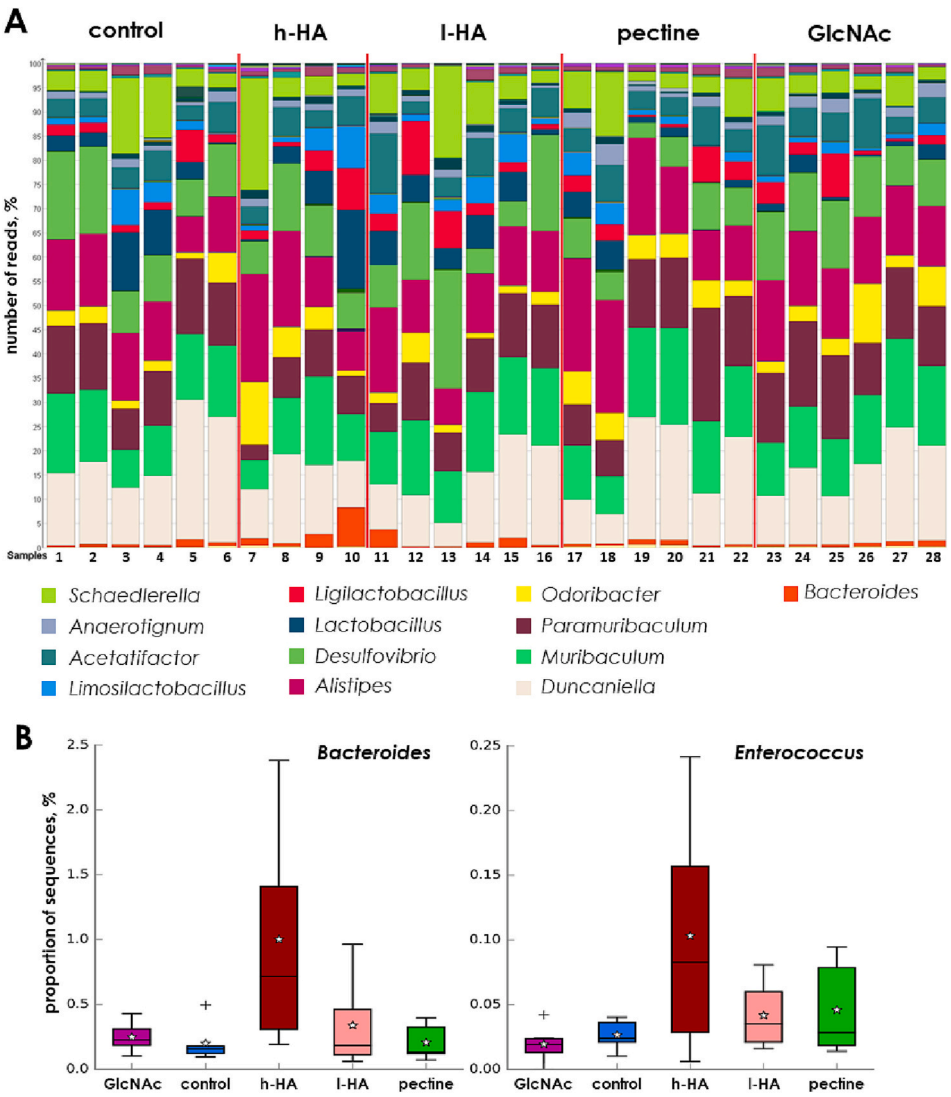

Fig. 6. Modulation of cecal microbiota by long-term HA-supplementation. A) Structural comparison of cecal microbiota at the genus level, B) Relative abundance of *Bacteroides* and *Enterococcus* in mice cecum after four-week supplementation with high doses of high-M_w HA (h-HA, 1600 kDa, 760 mg kg^{-1} day^{-1}), low doses of high-M_w HA (l-HA, 1600 kDa, 90 mg kg^{-1} day^{-1}), pectin (640 mg kg^{-1} day^{-1}) and GlcNAc (650 mg kg^{-1} day^{-1}).

show that the gut microbiota of conventional WT mice metabolize >97 % of administered high-M_w HA, and around 0.2 % is absorbed into the body of WT mice. Through the action of gut microbiota, M_w of high-M_w HA decreased into HA fragments of several kDa, and unsaturated oligosaccharides (mostly disaccharide) were formed. In contrast, only a slight decrease in the M_w of HA (1600 kDa → ~150–600 kDa) caused by acid hydrolysis in the stomach was observed for GF mice; nor were any unsaturated oligosaccharides typical for the activity of microbial HA lyases observed in the same mice. We identified ΔAN2 (0.38 kDa) as the dominant form of HA absorbed into the body, although the M_w cut-off for absorption of HA from the GIT was around 3 kDa. The degradation of HA by the well-defined gut microbiota mixture oMM[12] was tested *in vitro* and several biologically active metabolites including SCFA and UDP-GlcNAc were identified. However, metabolomic analyses showed that only unsaturated oligosaccharides and SCFA were available to the host *in vivo*. The *Bacteroides* genus metabolized high-M_w HA to ΔAN2 and SCFA *in vitro*. *In vivo*, long-term HA supplementation revealed an increase of *Bacteroides* abundance in the cecal content of conventional WT mice. These data show that *Bacteroides* could be an important player in the bioavailability of orally-administered high-M_w HA. Moreover, the limited absorption of orally-administered HA and its rapid metabolization by gut microbiota indicate that the *in vivo* fate of HA is not related to the M_w of the administered HA (15–1600 kDa) and that the orally-administered HA do not serve as an nutrition for joint and skin but its mechanism of action is probably the result of the systematic regulatory function of HA or its metabolites. However, to fully understand the mechanism of action of orally-applied HA directed at diseases of the extracellular matrix in distal tissues (skin, joints), further investigation of the interactions of oral HA with HA receptors and of the biological properties of unsaturated oligosaccharides is needed.

CRediT authorship contribution statement

Matěj Šimek: Conceptualization, Supervision, Visualization, Formal analysis, Data curation, Writing – original draft, Project administration. **Kristýna Turková:** Investigation, Data curation, Writing – original draft, Writing – review & editing. **Martin Schwarzer:** Visualization, Investigation, Conceptualization, Writing – review & editing. **Kristina Nešporová:** Conceptualization, Supervision. **Lukáš Kubala:** Funding acquisition, Supervision, Methodology, Resources, Writing – original draft, Project administration. **Martina Hermannová:** Supervision, Project administration. **Tereza Foglová:** Investigation. **Barbora Šafránková:** Investigation, Data curation. **Martin Šindelář:** Methodology, Data curation, Visualization. **Dagmar Šrůtková:** Investigation.

Sofia Chatzigeorgiou: Investigation. **Tereza Novotná:** Investigation. **Tomáš Hudcovic:** Methodology, Investigation. **Vladimír Velebný:** Funding acquisition, Supervision, Resources.

Declaration of competing interest

The authors declare no competing interests.

Data availability

Data will be made available on request.

Acknowledgements

This work was supported by the European Regional Development Fund - Project INBIO (No. CZ.02.1.01/0.0/0.0/16_026/0008451). MSch lab was supported by the Czech Science Foundation JUNIOR STAR grant (GAČR 21-19640M). The authors thank Dr. Martina Marchetti-Deschmann for the opportunity to measure MALDI-MS images in her laboratory at the Technical University of Vienna.

Appendix A. Supplementary data

Supplementary data to this article can be found online at https://doi.org/10.1016/j.carbpol.2023.120880.

References

Asari, A., Kanemitsu, T., & Kurihara, H. (2010). Oral administration of high molecular weight hyaluronan (900 kDa) controls immune system via toll-like receptor 4 in the intestinal epithelium. *Journal of Biological Chemistry, 285*(32), 24751–24758. https://doi.org/10.1074/jbc.M110.104950

Balogh, L., Polyak, A., Mathe, D., Kiraly, R., Thuroczy, J., Terez, M., Janoki, G., Ting, Y., Bucci, L. R., & Schauss, A. G. (2008). Absorption, uptake and tissue affinity of high-molecular-weight hyaluronan after oral administration in rats and dogs. *Journal of Agricultural and Food Chemistry, 56*(22), 10582–10593. https://doi.org/10.1021/jf8017029

Bellar, A., Kessler, S. P., Obery, D. R., Sangwan, N., Welch, N., Nagy, L. E., Dasarathy, S., & de la Motte, C. (2019). Safety of hyaluronan 35 in healthy human subjects: A pilot study. *Nutrients, 11*(5), 5. https://doi.org/10.3390/nu11051135

Biwi, J., Biot, C., Guerardel, Y., Vercoutter-Edouart, A.-S., & Lefebvre, T. (2018). The many ways by which O-GlcNAcylation may orchestrate the diversity of complex glycosylations. *Molecules, 23*(11), 11. https://doi.org/10.3390/molecules23112858

Blundell, C. D., & Almond, A. (2006). Enzymatic and chemical methods for the generation of pure hyaluronan oligosaccharides with both odd and even numbers of monosaccharide units. *Analytical Biochemistry, 353*(2), 236–247. https://doi.org/10.1016/j.ab.2006.03.013

Bouga, H., Tsouros, I., Bounias, D., Kyriakopoulou, D., Stavropoulos, M. S., Papageorgakopoulou, N., Theocharis, D. A., & Vynios, D. H. (2010). Involvement of hyaluronidases in colorectal cancer. *BMC Cancer, 10*(1), 499. https://doi.org/10.1186/1471-2407-10-499

Chaaban, H., Burge, K., Eckert, J., Trammell, M., Dyer, D., Keshari, R. S., Silasi, R., Regmi, G., Lupu, C., Good, M., McElroy, S. J., & Lupu, F. (2021). Acceleration of small intestine development and remodeling of the microbiome following hyaluronan 35 kDa treatment in neonatal mice. *Nutrients, 13*(6), 6. https://doi.org/10.3390/nu13062030

Chowdhury, B., Hemming, R., Faiyaz, S., & Triggs-Raine, B. (2016). Hyaluronidase 2 (HYAL2) is expressed in endothelial cells, as well as some specialized epithelial cells, and is required for normal hyaluronan catabolism. *Histochemistry and Cell Biology, 145*(1), 53–66.

Cowman, M. K., Lee, H.-G., Schwertfeger, K. L., McCarthy, J. B., & Turley, E. A. (2015). The content and size of hyaluronan in biological fluids and tissues. *Frontiers in Immunology, 6*. https://doi.org/10.3389/fimmu.2015.00261

Čožíková, D., Šílová, T., Moravcová, V., Šmejkalová, D., Pepeliaev, S., Velebný, V., et al. (2017). Preparation and extensive characterization of hyaluronan with narrow molecular weight distribution. *Carbohydrate Polymers, 160*, 134–142. https://doi.org/10.1016/j.carbpol.2016.12.045

de Souza, A. B., Chaud, M. V., & Santana, M. H. A. (2019). Hyaluronic acid behavior in oral administration and perspectives for nanotechnology-based formulations: A review. *Carbohydrate Polymers, 222*, Article 115001. https://doi.org/10.1016/j.carbpol.2019.115001

Eberl, C., Ring, D., Münch, P. C., Beutler, M., Basic, M., Slack, E. C., Schwarzer, M., Srutkova, D., Lange, A., Frick, J. S., Bleich, A., & Stecher, B. (2020). Reproducible colonization of germ-free mice with the oligo-mouse-microbiota in different animal facilities. *Frontiers in Microbiology, 10*. https://doi.org/10.3389/fmicb.2019.02999

Gracz, A. D., Fuller, M. K., Wang, F., Li, L., Stelzner, M., Dunn, J. C. Y., Martin, M. G., & Magness, S. T. (2013). Brief report: CD24 and CD44 mark human intestinal epithelial cell populations with characteristics of active and facultative stem cells. *Stem Cells, 31*(9), 2024–2030. https://doi.org/10.1002/stem.1391

Gupta, R. C., Lall, R., Srivastava, A., & Sinha, A. (2019). Hyaluronic acid: Molecular mechanisms and therapeutic trajectory. *Frontiers in Veterinary Science, 6*, 192. https://doi.org/10.3389/fvets.2019.00192

Han, W., Song, L., Wang, Y., Lv, Y., Chen, X., & Zhao, X. (2019). Preparation, characterization, and inhibition of hyaluronic acid oligosaccharides in triple-negative breast cancer. *Biomolecules, 9*(9), 9. https://doi.org/10.3390/biom9090436

Hisada, N., Satsu, H., Mori, A., Totsuka, M., Kamei, J., Nozawa, T., & Shimizu, M. (2008). Low-molecular-weight hyaluronan permeates through human intestinal Caco-2 cell monolayers via the paracellular pathway. *Bioscience, Biotechnology, and Biochemistry, 72*(4), 1111–1114.

Johansson, M. E. V., Jakobsson, H. E., Holmén-Larsson, J., Schütte, A., Ermund, A., Rodríguez-Piñeiro, A. M., Arike, L., Wising, C., Svensson, F., Bäckhed, F., & Hansson, G. C. (2015). Normalization of host intestinal mucus layers requires long-term microbial colonization. *Cell Host & Microbe, 18*(5), 582–592. https://doi.org/10.1016/j.chom.2015.10.007

Kawada, C., Yoshida, T., Yoshida, H., Matsuoka, R., Sakamoto, W., Odanaka, W., Sato, T., Yamasaki, T., Kanemitsu, T., Masuda, Y., & Urushibata, O. (2014). Ingested hyaluronan moisturizes dry skin. *Nutrition Journal, 13*(1), 70. https://doi.org/10.1186/1475-2891-13-70

Kawai, K., Kamochi, R., Oiki, S., Murata, K., & Hashimoto, W. (2018). Probiotics in human gut microbiota can degrade host glycosaminoglycans. *Scientific Reports, 8*(1), 10674. https://doi.org/10.1038/s41598-018-28886-w

Kessler, S. P., Obery, D. R., Nickerson, K. P., Petrey, A. C., McDonald, C., & de la Motte, C. A. (2018). Multifunctional role of 35 kilodalton hyaluronan in promoting defense of the intestinal epithelium. *Journal of Histochemistry & Cytochemistry.*. https://doi.org/10.1369/0022155417746775

Kim, Y., & de la Motte, C. A. (2020). The role of hyaluronan treatment in intestinal innate host defense. *Frontiers in Immunology, 11*, 569. https://doi.org/10.3389/fimmu.2020.00569

Kim, Y., West, G. A., Ray, G., Kessler, S. P., Petrey, A. C., Fiocchi, C., McDonald, C., Longworth, M. S., Nagy, L. E., & de la Motte, C. A. (2018). Layilin is critical for mediating hyaluronan 35kDa-induced intestinal epithelial tight junction protein ZO-1 in vitro and in vivo. *Matrix Biology, 66*, 93–109. https://doi.org/10.1016/j.matbio.2017.09.003

Kobayashi, T., Chanmee, T., & Itano, N. (2020). Hyaluronan: Metabolism and function. *Biomolecules, 10*(11), 11. https://doi.org/10.3390/biom10111525

Kolar, S. L., Kyme, P., Tseng, C. W., Soliman, A., Kaplan, A., Liang, J., Nizet, V., Jiang, D., Murali, R., Arditi, M., Underhill, D. M., & Liu, G. Y. (2015). Group B streptococcus evades host immunity by degrading hyaluronan. *Cell Host & Microbe, 18*(6), 694–704. https://doi.org/10.1016/j.chom.2015.11.001

Körver-Keularts, I. M. L. W., Wang, P., Waterval, H. W. A. H., Kluijtmans, L. A. J., Wevers, R. A., Langhans, C.-D., Scott, C., Habets, D. D. J., & Bierau, J. (2018). Fast and accurate quantitative organic acid analysis with LC-QTOF/MS facilitates screening of patients for inborn errors of metabolism. *Journal of Inherited Metabolic Disease, 41*(3), 415–424. https://doi.org/10.1007/s10545-017-0129-0

Laznicek, M., Laznickova, A., Cozikova, D., & Velebny, V. (2012). Preclinical pharmacokinetics of radiolabeled hyaluronan. *Pharmacological Reports, 64*(2), 428–437. https://doi.org/10.1016/S1734-1140(12)70784-3

Lee, Y., Sugihara, K., Gillilland, M. G., Jon, S., Kamada, N., & Moon, J. J. (2020). Hyaluronic acid–bilirubin nanomedicine for targeted modulation of dysregulated intestinal barrier, microbiome and immune responses in colitis. *Nature Materials, 19*(1), 118–126. https://doi.org/10.1038/s41563-019-0462-9

Luczynski, P., McVey Neufeld, K.-A., Oriach, C. S., Clarke, G., Dinan, T. G., & Cryan, J. F. (2016). Growing up in a bubble: Using germ-free animals to assess the influence of the gut microbiota on brain and behavior. *The International Journal of Neuropsychopharmacology, 19*(8), pyw020. https://doi.org/10.1093/ijnp/pyw020

Ma, W., Wang, J., Guo, Q., & Tu, P. (2015). Quantitative subcellular study of doxorubicin in MCF-7/Adr cells using liquid chromatography–tandem mass spectrometry. *Journal of Chromatography B, 1007*, 18–22. https://doi.org/10.1016/j.jchromb.2015.11.002

Mao, T., Su, C.-W., Ji, Q., Chen, C.-Y., Wang, R., Vijaya Kumar, D., Lan, J., Jiao, L., & Shi, H. N. (2021). Hyaluronan-induced alterations of the gut microbiome protects mice against Citrobacter rodentium infection and intestinal inflammation. *Gut Microbes, 13*(1), 1972757. https://doi.org/10.1080/19490976.2021.1972757

McConnell, E. L., Basit, A. W., & Murdan, S. (2008). Measurements of rat and mouse gastrointestinal pH, fluid and lymphoid tissue, and implications for in-vivo experiments. *Journal of Pharmacy and Pharmacology, 60*(1), 63–70. https://doi.org/10.1211/jpp.60.1.0008

McKee, L. S., La Rosa, S. L., Westereng, B., Eijsink, V. G., Pope, P. B., & Larsbrink, J. (2021). Polysaccharide degradation by the Bacteroidetes: Mechanisms and nomenclature. *Environmental Microbiology Reports, 13*(5), 559–581. https://doi.org/10.1111/1758-2229.12980

Ndeh, D., Baslé, A., Strahl, H., Yates, E. A., McClurgg, U. L., Henrissat, B., Terrapon, N., & Cartmell, A. (2020). Metabolism of multiple glycosaminoglycans by Bacteroides thetaiotaomicron is orchestrated by a versatile core genetic locus. *Nature Communications, 11*(1), 1. https://doi.org/10.1038/s41467-020-14509-4

Oe, M., Mitsugi, K., Odanaka, W., Yoshida, H., Matsuoka, R., Seino, S., Kanemitsu, T., & Masuda, Y. (2014). Dietary hyaluronic acid migrates into the skin of rats. *The Scientific World Journal, 2014*, Article 378024. https://doi.org/10.1155/2014/378024

Oe, M., Tashiro, T., Yoshida, H., Nishiyama, H., Masuda, Y., Maruyama, K., Koikeda, T., Maruya, R., & Fukui, N. (2016). Oral hyaluronan relieves knee pain: A review. *Nutrition Journal, 15*, 11. https://doi.org/10.1186/s12937-016-0128-2

Oiki, S., Mikami, B., Maruyama, Y., Murata, K., & Hashimoto, W. (2017). A bacterial ABC transporter enables import of mammalian host glycosaminoglycans. *Scientific Reports, 7*(1), 1069. https://doi.org/10.1038/s41598-017-00917-y

Pan, L., Ai, X., Fu, T., Ren, L., Shang, Q., Li, G., & Yu, G. (2021). In vitro fermentation of hyaluronan by human gut microbiota: Changes in microbiota community and potential degradation mechanism. *Carbohydrate Polymers, 269*, Article 118313. https://doi.org/10.1016/j.carbpol.2021.118313

Parada Venegas, D., De la Fuente, M. K., Landskron, G., González, M. J., Quera, R., Dijkstra, G., Harmsen, H. J. M., Faber, K. N., & Hermoso, M. A. (2019). Short chain fatty acids (SCFAs)-mediated gut epithelial and immune regulation and its relevance for inflammatory bowel diseases. *Frontiers in Immunology, 10*. https://doi.org/10.3389/fimmu.2019.00277

Reichardt, N., Duncan, S. H., Young, P., Belenguer, A., McWilliam Leitch, C., Scott, K. P., Flint, H. J., & Louis, P. (2014). Phylogenetic distribution of three pathways for propionate production within the human gut microbiota. *The ISME Journal, 8*(6), 1323–1335. https://doi.org/10.1038/ismej.2014.14

Rodrigues, M. T., Carvalho, P. P., Gomes, M. E., & Reis, R. L. (2015). Chapter 11—Biomaterials in preclinical approaches for engineering skeletal tissues. In A. Atala, & J. G. Allickson (Eds.), *Translational Regenerative Medicine* (pp. 127–139). Academic Press. https://doi.org/10.1016/B978-0-12-410396-2.00011-6.

Sato, Y., Joumura, T., Takekuma, Y., & Sugawara, M. (2020). Transfer of orally administered hyaluronan to the lymph. *European Journal of Pharmaceutics and Biopharmaceutics, 154*, 210–213. https://doi.org/10.1016/j.ejpb.2020.07.007

Shi, X., Wang, S., Jasbi, P., Turner, C., Hrovat, J., Wei, Y., Liu, J., & Gu, H. (2019). Database-assisted globally optimized targeted mass spectrometry (dGOT-MS): Broad and reliable metabolomics analysis with enhanced identification. *Analytical Chemistry, 91*(21), 13737–13745. https://doi.org/10.1021/acs.analchem.9b03107

Shimizu, K., Seiki, I., Goto, Y., & Murata, T. (2021). Measurement of the intestinal pH in mice under various conditions reveals alkalization induced by antibiotics. *Antibiotics, 10*(2), 180.

Šimek, M., Hermannová, M., Šmejkalová, D., Foglová, T., Souček, K., Binó, L., & Velebný, V. (2019). LC–MS/MS study of in vivo fate of hyaluronan polymeric micelles carrying doxorubicin. *Carbohydrate Polymers*, 181–189. https://doi.org/10.1016/j.carbpol.2018.12.104

Šimek, M., Nešporová, K., Kocurková, A., Foglová, T., Ambrožová, G., Velebný, V., Kubala, L., & Hermannová, M. (2021). How the molecular weight affects the in vivo fate of exogenous hyaluronan delivered intravenously: A stable-isotope labelling strategy. *Carbohydrate Polymers, 263*, Article 117927. https://doi.org/10.1016/j.carbpol.2021.117927

Sindelar, M., Jilkova, J., Kubala, L., Velebny, V., & Turkova, K. (2021). Hyaluronidases and hyaluronate lyases: From humans to bacteriophages. *Colloids and Surfaces B: Biointerfaces, 208*, Article 112095. https://doi.org/10.1016/j.colsurfb.2021.112095

Soroosh, A., Albeiroti, S., West, G. A., Willard, B., Fiocchi, C., & de la Motte, C. A. (2016). Crohn's disease fibroblasts overproduce the novel protein KIAA1199 to create proinflammatory hyaluronan fragments. *Cellular and Molecular Gastroenterology and Hepatology, 2*(3), 358–368.e4. https://doi.org/10.1016/j.jcmgh.2015.12.007

Štěpánková, R., Tlaskalová-hogenová, H., Šinkora, J., Jodl, J., & Frič, P. (1996). Changes in jejunal mucosa after long-term feeding of germfree rats with gluten. *Scandinavian Journal of Gastroenterology, 31*(6), 551–557. https://doi.org/10.3109/00365529609009127

Stern, R., Kogan, G., Jedrzejas, M. J., & Šoltés, L. (2007). The many ways to cleave hyaluronan. *Biotechnology Advances, 25*(6), 537–557. https://doi.org/10.1016/j.biotechadv.2007.07.001

Svanovsky, E., Velebny, V., Laznickova, A., & Laznicek, M. (2008). The effect of molecular weight on the biodistribution of hyaluronic acid radiolabeled with111In after intravenous administration to rats. *European Journal of Drug Metabolism and Pharmacokinetics, 33*(3), 149–157. https://doi.org/10.1007/BF03191112

Uhlén, M., Fagerberg, L., Hallström, B. M., Lindskog, C., Oksvold, P., Mardinoglu, A., Sivertsson, Å., Kampf, C., Sjöstedt, E., Asplund, A., Olsson, I., Edlund, K., Lundberg, E., Navani, S., Szigyarto, C. A.-K., Odeberg, J., Djureinovic, D., Takanen, J. O., Hober, S.Pontén, F., … (2015). Tissue-based map of the human proteome. *Science, 347*(6220), 1260419. https://doi.org/10.1126/science.1260419

Volpi, N. (2002). Oral bioavailability of chondroitin sulfate (Condrosulf®) and its constituents in healthy male volunteers. *Osteoarthritis and Cartilage, 10*(10), 768–777. https://doi.org/10.1053/joca.2002.0824

Volpi, N. (2003). Oral absorption and bioavailability of ichthyic origin chondroitin sulfate in healthy male volunteers. *Osteoarthritis and Cartilage, 11*(6), 433–441. https://doi.org/10.1016/S1063-4584(03)00051-7

Wu, W. M., Yang, Y. S., & Peng, L. H. (2014). Microbiota in the stomach: New insights. *Journal of Digestive Diseases, 15*(2), 54–61. https://doi.org/10.1111/1751-2980.12116

Yilmaz, B., Mooser, C., Keller, I., Li, H., Zimmermann, J., Bosshard, L., Fuhrer, T., Gomez de Agüero, M., Trigo, N. F., Tschanz-Lischer, H., Limenitakis, J. P., Hardt, W.-D., McCoy, K. D., Stecher, B., Excoffier, L., Sauer, U., Ganal-Vonarburg, S. C., & Macpherson, A. J. (2021). Long-term evolution and short-term adaptation of microbiota strains and sub-strains in mice. *Cell Host & Microbe, 29*(4), 650–663.e9. https://doi.org/10.1016/j.chom.2021.02.001